A POWER-BALANCE MODEL OF DENSITY LIMIT IN FUSION PLASMAS

P. Zanca, F. Sattin
Consorzio RFX (CNR, ENEA, INFN, Università di Padova, Acciaierie Venete Spa)
Padova, Italy.
Email: paolo.zanca@igi.cnr.it

D. F. Escande
Aix-Marseille Université, CNRS, PIIM
Marseille, France.

JET Contributors: see the author list of "X. Litaudon et al 2017 Nucl. Fusion 57 102001"

Abstract

A power-balance model, with radiation losses from impurities and neutrals, gives a unified description of density limit in L-mode tokamak, stellarator and Reversed Field Pinch. The model is compared to experimental data from high-density disrupted-L-mode discharges performed at JET.

1. INTRODUCTION

A density limit (DL), causing either a disruption or a soft termination of the discharge, is generally found in magnetic confinement fusion devices. Some empirical scaling laws have been proposed to order the maximum achievable densities. The Sudo density, $n_{Sudo} \propto \left(P\ B_\phi\right)^{0.5}$ [1], with P the total heating power, is generally applied to the stellarator. The Greenwald density, $n_G(10^{20}m^{-3}) = I_p(MA)/(\pi a^2)$ [2], being a the minor radius of the device, and I_p the plasma current, represents a reference for the ohmic tokamak and the Reversed Field Pinch (RFP): a remarkable feature given the differences of these two configurations both in terms of magnetic profiles and transport properties. Additionally heated tokamak experiments in L-mode suggest dependences approximately of the form $P^{0.3\div0.5}I_p^{0.5}$ [3, 4]. The tokamak H-mode DL, identified by a back transition to L-mode and therefore not disruptive in general, seems to be more device dependent: in particular, no dependence on P is found in [5], whereas a dependence $P^{0.4}$ is obtained in [6]. We present a basic power-balance model [7], providing a unified interpretation of DL in the stellarator, in the L-mode tokamak and in the RFP. In fact, scaling laws resembling the above empirical trends, but richer in their parametric dependence, are derived as special cases of a more fundamental relation, which delimits the thermal equilibrium states having realistic temperature profiles (i.e. with low temperature only at the edge) in the presence of radiation losses. The model describes, better than the pure Greenwald limit, high-density disrupted L-mode experiments performed at JET. With respect to previous validations based on published data [7], here we take advantage of shot-by-shot signals for most of the needed quantities, obtained by access to the experimental pulse-files.

2. THE MODEL

Two refinements are added to the previous analytical model [7]: 1) inclusion of radiation from the plasma bulk, in addition to that from the edge; 2) replacement of thermal conductivity by the global energy confinement time τ_E in the final DL scaling laws. We also refer to [8] for some specific analysis, which the limited space of this paper does not allow to present. The starting point is a phenomenological equation describing thermal balance in cylindrical geometry, obtained by adding the heat transport equations for electrons and main ions and neglecting convection as well as viscous heating:

$$1)\ \frac{d}{dr}\left(r\ K\ \frac{dT}{dr}\right) + r(\wp - \Re)\ = 0; \quad \Re = \ n_e^2\left[\sum_j f_j Rad_j\ (T) + f_0 Rad_0(T) + Rad_i(T)\right]$$

Here, T is the electron temperature, K is an effective perpendicular conductivity, which includes the main ion contribution to the heat flux [7], and $\wp$, $\Re$ are respectively the total heating power density (with ohmic and auxiliary components) and the radiated power density. Moreover, n_e is the electron density, f_j, Rad_j are the j-th impurity concentration and radiative loss rate respectively, and f_0, Rad_0 are the same quantities for neutrals. Finally, Rad_i is the main ion radiative loss rate, a minor effect in the plasmas here considered. The impurity concentrations are allowed to vary with r, but the concentrations relative to the dominant impurity (denoted by d),

$\hat{f}_j = f_j/f_d$, *are assumed to be radially constant*. Throughout this paper we use the International System of units (SI), but for the temperature, which is expressed in keV. Therefore, *K* incorporates the numerical factor 1.6×10^{-16}. The temperature profile satisfies the symmetry condition $T'(0) = 0$ ($'\equiv d/dr$). Moreover, the request of ambient temperature value at *r*=*a*, location of the material boundary, is modelled by the constraint *T*(*a*)=0. For a plasma mainly polluted by light impurities the loss term $\sum_j f_j Rad_j$ peaks at low temperature (order tens eV): schematically, we can distinguish the *edge radiation*, affecting the low temperature region $T < T_*$ where the above term peaks, from the *bulk radiation*, affecting the region $T > T_*$. The separation radius r_*, defined by $T(r_*) = T_*$, is assumed to be uniquely determined and close to the wall: $r_* \approx a$. Given the smallness of T_*, these two hypotheses should apply to a realistic temperature profile. Neutral particles are considered *only at the edge* with constant f_0: $f_0 = \{f_{0*},\ r > r_*;\quad 0,\ r < r_*\}$. In order to have an order-of-magnitude assessment of their radiated power, we consider atomic D_0 line emission only: the inclusion of other loss mechanisms can be simulated by increasing f_{0*}. Hence, f_{0*} should be considered an *effective concentration parameter*. Though $r_* \approx a$, we have to distinguish the temperature derivatives at *a* and r_*, since a finite variation of T' occurs across the edge radiative layer, due to the peaking of $\Re$ therein. It is convenient defining an *impurity-average loss rate* F, such that $\sum_j f_j Rad_j = \left(Z_{eff} - Z_i\right) \times F$, with the plasma effective charge $Z_{eff} = Z_i + \sum_j f_j\left(Z_j^2 - Z_j Z_i\right)$ taken *radially constant*; Z_i, $Z_j(T)$, denote main ion and impurities charges respectively. Hence, $F(T, \hat{f}_j) = \sum_j \hat{f}_j Rad_j(T) / \sum_j \hat{f}_j\left[Z_j^2(T) - Z_j(T) Z_i\right]$. The total radiated power is split into edge and bulk contributions, expressed by temperature integrals of loss rates in these two regions and by two suitable densities n_*, n_{bulk} *representative* of the edge and bulk respectively:

$$2)\ \int_0^a dr\ r\ \Re \cong \frac{a^2}{2} n_{bulk}^2 \mathrm{H}_{bulk} - \frac{a}{X}\ n_*^2\ \mathrm{G}_*; \qquad \mathrm{H}_{bulk} = \frac{\int_{T_*}^{T_0} Rad_i dT\ +\ (Z_{eff} - Z_i) \int_{T_*}^{T_0} F\ dT}{T_0 - T_*};$$

$$T_0 = T(0); \quad X = [T'(a) + T'(r_*)]/2; \quad \mathrm{G}_* = f_{0*} \int_0^{T_*} Rad_0\ dT + \left(Z_{eff} - Z_i\right) \int_0^{T_*} F\ dT$$

Then, we consider the half-sum of the integrals of (1) over $[0, a]$ and $[0, r_*]$. One gets a second-order algebraic equation for *X*: $2\ K_* X^2 + a[\langle \wp \rangle - n_{bulk}^2 H_{bulk}] X + n_*^2 G_* = 0$. Here $\langle\ \ \rangle$ denotes volume average, and $K_* = K(r_*) \approx K(a)$. The discriminant is positive or zero, and there are real-valued negative solutions for *X*, when $a[\langle \wp \rangle - n_{bulk}^2 H_{bulk}] \geq (8 K_* G_*)^{\frac{1}{2}}\ n_*$. We explicit the DL embedded in this condition by introducing the profile factor $\delta_n = n_{bulk}/n_*$, and the two densities $n_H^2 = \langle \wp \rangle / H_{bulk}$, $n_L = a\langle \wp \rangle / (8 K_* G_*)^{\frac{1}{2}}$, with the following meaning: n_H is the DL for n_{bulk} in the absence of edge radiation ($G_* = 0$); n_L is the DL for n_* in the absence of bulk radiation ($H_{bulk} = 0$). After a little algebra, the DL condition can be cast into the form

$$3)\ n_* \leq n_L \times \Theta(\iota); \qquad \Theta(\iota) = \left[(1 + 2\iota)^{\frac{1}{2}} - 1\right]/\iota; \qquad \iota = 2\delta_n^2 n_L^2 / n_H^2;$$

where Θ weighs the contributions of edge and bulk radiations: if edge radiation is dominant, then $\iota \ll 1$, $\Theta \approx 1$, and $n_* \approx n_L$; if bulk radiation is dominant, then $\iota \gg 1$, $\Theta \approx (2/\iota)^{1/2}$, and $n_{bulk} \approx n_H$ Finally, we note that $T'(a) = 0$ when the above discriminant equals zero, i.e. when (3) is satisfied as equality: in this somewhat idealized model the DL corresponds to the condition of vanishing heat flux at the edge, implying total heating power equal to total radiated power. We will now further develop (3), by providing more explicit expressions for n_H and n_L. It is convenient writing $n_H(10^{20} m^{-3}) = \left[P(MW) / \left(V \hat{H}_{bulk}\right)\right]^{1/2}$, being $\hat{H}_{bulk} = 10^{34} \times H_{bulk}$ and $V = 2\pi^2 R_0 a^2$ the plasma volume, with R_0 the major radius. In order to manage n_L, we express the edge conductivity K_* in terms of τ_E and a suitable profile factor. We start from the *operative definition* of τ_E in stationary conditions [10]: $\tau_E = 1.6 \times 10^{-16} \times 3V\langle n_e T \rangle / P = 4.8 \times 10^{-16} V\ \delta_n\ \delta_{nT}\ n_* T_0 / P$, being $\delta_{nT} = \langle n_e / n_{bulk} \times T / T_0 \rangle$ a profile factor (the approximation made here of taking same temperature for electrons and main ions has little impact due to the weak dependence on τ_E of the final DL scaling laws, as we shall see). This definition is combined with an equation for T_0 obtained from (1) integrated twice, first over $[0, r]$, then over $[0, a]$ after a division by *r*. Under DL conditions $\int_0^a dr\ r\ (\wp - \Re) = 0$, we factor the total heating power (equal to the total radiated power), with radial profiles encapsulated into the integral $\Im_p$:

$$4)\ K_* T_0 = \frac{P}{4\pi^2 R_0} \Im_p; \quad \Im_p = \int_0^a dr \frac{1}{r\ \bar{K}} \left(\frac{\int_0^r dy\ y\ \hat{\wp}}{\int_0^a dy\ y\ \hat{\wp}} - \frac{\int_0^r dy\ y\ \hat{\Re}}{\int_0^a dy\ y\ \hat{\Re}} \right); \ \bar{K} = K/K_*; \ \hat{\wp} = \wp/\wp(0); \ \hat{\Re} = \Re/\Re(r_*)$$

Hence,

5) $K_* = 2.4 \times 10^{-16}\, a^2 n_*/\tau_E\, \Psi_p, \qquad \Psi_p = \delta_n \delta_{nT} \Im_p,$

being Ψ_p a further profile factor. Finally, in terms of τ_E the expression of n_L becomes

6) $n_L(10^{20} m^{-3}) = 0.51 \times \left[\frac{P(MW)}{a^2 R_0}\right]^{\frac{2}{3}} \left[\frac{\tau_E}{\hat{G}_* \Psi_p \Theta(\iota)}\right]^{\frac{1}{3}}; \qquad \hat{G}_* = 10^{35} \times G_*$

Note that it is an implicit relation (since $\iota = 2\delta_n^2 n_L^2/n_H^2$) to be solved iteratively, after computing n_H. Factor Ψ_p mainly depends on the thermal conductivity radial profile, and it is estimated by numerical solutions of equation (1) written for normalized quantities [8]. Expression (6) can be applied to any magnetic configuration, by specializing τ_E and Ψ_p. We provide two examples: the L-mode tokamak and the stellarator. Moreover, we also derive a Greenwald-like expression from (6), having a tenuous dependence on τ_E.

2.1 $\mathbf{n_L}$ for the L-mode tokamak

Setting in (6) the ITER89-P scaling law, including the atomic mass *A* and the elongation κ, $\tau_E^{ITER89-P}(s) = 0.048 \times I_p(MA)^{0.85} B_\phi^{0.2} P(MW)^{-0.5} (n_{bulk}/10^{20})^{0.1}\ R_0^{1.5} (a/R_0)^{0.3}\ (A\ \kappa)^{0.5}$, one gets:

7) $n_L(10^{20} m^{-3}) \cong 0.175 \times P(MW)^{0.517}\ I_p(MA)^{0.293}\ B_\phi^{0.069}\ R_0^{-0.276}\ a^{-1.276}\ \left[\hat{G}_*\ \Psi_p\ \Theta(i)\right]^{-0.345} (A\ \kappa)^{0.173}$

With respect to (6), the power dependence reduces from $P^{2/3}$ to $\sim P^{0.5}$, and the current dependence $\sim I_p^{0.3}$ appears. With a radially increasing thermal diffusivity ($= K/n_e$), suggested by experimental transport analysis in L mode [11], one also gets $\Psi_p^{-0.345} \approx 2.83 \times \delta_T^{0.529}\ \delta_n^{-0.321} \delta_{Rad}^{0.269}$ [8], being $\delta_T = \langle T/T(0) \rangle$ a temperature shape factor, and $\delta_{Rad} = \int_0^1 dx x \Re / \int_0^{x_*} dx x \Re = 1 + [T_*/2(1 - x_*)] \delta_n^2 H_{bulk}/G_*$ a radiation shape factor, to express which use is made of (2) and approximation $T_* \approx (r_* - a)X$.

2.2 $\mathbf{n_L}$ for the Stellarator

Replacing in (6) the International Stellarator scaling 95, including the rotational transform ι at $r = 2/3\, a$, $\tau_E^{ISS95}(s) = 0.079 \times B_\phi^{0.83} P(MW)^{-0.59}\ (n_{bulk}/10^{19})^{0.51}\ a^{2.21} R_0^{0.65}\ \iota^{0.4}$, a Sudo-like scaling is obtained:

8) $n_L(10^{20} m^{-3}) \cong 0.257 \times P(MW)^{0.566}\ B_\phi^{0.334}\ R_0^{-0.542}\ a^{-0.718}\ \left[\hat{G}_*\ \Psi_p\ \right]^{-0.4} \Theta(i)^{-0.197}\ \iota^{0.16} \delta_n^{0.2}$

With a non-monotonic fixed parabolic profile for the thermal diffusivity, approximating the LHD experimental estimates [12], one gets $\Psi_p^{-0.4} \approx 3.62 \times \delta_T^{0.544}\ \delta_n^{-0.396}\ \delta_{Rad}^{0.375}$. Then, (8) turns out be almost equivalent to the DL scaling laws derived in [7] for the stellarator case in the pure edge radiation limit ($n_* = n_L$).

2.3 Greenwald-like form of $\mathbf{n_L}$

For tokamak and RFP we can also combine the ohmic component of P in (6) with the stationary, on-axis Ohm's law with Spitzer resistivity (neoclassical effects vanish at *r*=0):

9) $V_\phi = \eta_1\ \zeta\ Z_{eff}\ T_0^{-\frac{3}{2}} B_\phi(0)/q(0)\ \ \xi(0)\ \ C(0); \qquad \zeta = 0.58 + 0.74/\left(0.76 + Z_{eff}\right)$

Toroidal loop voltage is denoted by V_ϕ. Moreover, $\eta_1 = 0.0165 \times ln\Lambda$, being $ln\Lambda$ the Coulomb logarithm; $\xi(r) = J_\Omega/J$ is the current-drive function, with J, J_Ω the current density magnitude, total and ohmic respectively ($\xi = 1$, for RFP, meant as purely ohmic); $C(r) = E_\phi\ J_\phi/(\eta\ J^2)$ is the RFP anomaly function quantifying the dynamo process [13] ($C = 1$ for the tokamak). Making also use of (4) and (5), after some algebra one gets a Greenwald-like form for n_L, having *a negligible dependence on transport* ($\tau_E^{-1/9}$):

10) $n_L(10^{20}) = 0.425 \times \left(\eta_1 \zeta\ Z_{eff}\ \Pi\right)^{\frac{4}{9}}\ \ \hat{G}_*^{-\frac{5}{9}}\ \Psi^{\frac{10}{9}}\ [\Theta(\iota)/\tau_E]^{\frac{1}{9}} \times n_G^{\frac{8}{9}}; \qquad \Pi_{tok} = \xi(0) P/\left(V_\phi I_p\right);$

$$\Pi_{RFP} = \frac{1}{a\hat{B}_\phi(a)\hat{B}_\theta(a)} \int_0^a \frac{d}{dr}\left(r\hat{B}_\theta\right)\ \hat{C}^{-1}\ dr\ ;\quad \hat{C} = C/C(0);\quad \hat{\mathbf{B}} = \mathbf{B}/B_\phi(0);\quad \Psi = [q(a)/q(0)]^{\frac{2}{5}}\ \Im_p^{-\frac{3}{5}}\ \Psi_p^{\frac{1}{10}}$$

Ψ is a further profile factor. In particular, for the L-mode tokamak, the numerical analysis provides $\Psi \approx 4.43 \times \delta_T^{0.825}\ \delta_n^{0.166}\delta_{Rad}^{0.387}$. Quantity Π has different meanings for the tokamak and the RFP: respectively, power enhancement factor with respect to the pure ohmic heating, and profile factor for the anomaly function. Scaling (10) does not depend explicitly on P for the ohmic tokamak ($\Pi_{tok} = 1$) and the RFP. For the tokamak, note also the explicit total dependence $P^{4/9}\ I_p^{4/9}$, similar to that of (7).

3. JET L-MODE EXPERIMENTS: GENERAL FEATURES

This DL model is used to interpret L mode JET discharges, disrupted after a density ramp-up, without impurity seeding. We consider 10 discharges with carbon (C) wall (in D: 43161, 43547, 45479, 55539, 55541, 55543, 59648, 75673 76285; in He: 54000), and 5 discharges with beryllium-tungsten wall (Be-W) [14], all in D (81491, 82342, 86953, 86956, 87494). As far as interferometric data are concerned, only the on-axis value n_0 and the volume-average value $\langle n_e \rangle$ are available in the present database. Hence, the density profile shape factor is estimated by $\delta_n \sim n_0/\langle n_e \rangle$. The profiles are rather flat ($\delta_n < 1.5$), when density increases. Experimental $\langle n_e \rangle$ are compared to n_G in figure 1: *the full trace* of the considered quantities is displayed up to the disruption, excluding only the initial start-up phase, for the whole database. The cross-marks represent the time averages 1s before the disruption, where density reaches the maximum value. It is evident that n_G does not describe the upper boundary of the experimental densities. In the next paragraph we will compare $\langle n_e \rangle$ with the modelled $n_{bulk} = n_* \times \delta_n$. In order to compute n_* by (3), with n_L given either by (7) or by (10), some experimental quantities are needed, besides the straightforward $R_0 = 2.98m,\ a = 0.95m,\ A, \kappa, I_p$. First, the total heating power P: in addition to the ohmic input, estimated by V_ϕ and I_p (typically below 2MW), all of the present discharges feature NBI heating (some of them include a smaller ICRH input). However, in figure 2 one can appreciate that scaling (10) does not deviate significantly from the ohmic one ($\Pi_{tok}^{4/9} < 1.5$), in general. Due to several loss mechanisms, only a fraction of the NBI injected power contributes to P. The best we can do to quantify losses is adding the shine-through power, available as a pulse-file signal, to the fraction of power lost by charge-exchange and unconfined orbits, estimated by $0.01 \times exp\left[3.35 - 0.667/I_p(MA) - 0.2 \times \langle n_e \rangle (10^{19} m^{-3})\right]$ [15]. The computed losses are rather small, less than 20% when density increases. Furthermore, in order to obtain $\hat{H}_{bulk}$, $\hat{G}_*$ we need the functions $Z_j(T), Rad_j(T), Rad_i(T), Rad_0(T)$, which are taken from the database [9], the average Z_{eff}, available from visible bremsstrahlung, and T_0, T_*, $\hat{f}_j$, f_{0*}. Thomson scattering provides T_0, and we fix $T_* = 50eV$, benefiting of the weak dependence of (7), (10) on this parameter [8]. Parameters $\hat{f}_j$, f_{0*} are of more difficult assessment, but spectroscopic measurements give some indications. In particular, the choice of a sensible range for f_{0*} is guided by comparing the ratio $Q_*(f_{0*}) = \left(Z_{eff} - Z_i\right) \int_0^{T*} F dT \Big/ \left[f_{0*} \int_0^{T*} Rad_0 dT\right]$ between edge radiated powers from impurities and neutrals (see equation (2)), to scrape-off-layer (SOL) analyses [16]. Finally, shape factors δ_T, δ_{Rad}, entering in the approximations for Ψ_p, Ψ, need an estimate: δ_T is provided by Thomson scattering, δ_{Rad} is computed by fixing the further quantity $x_* = 0.9$ (see paragraph 2.1).

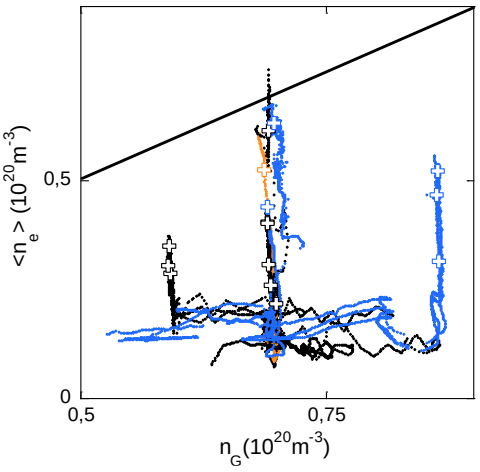

FIG. 1. Volume-average density versus n_G in the considered database (black: D with C-wall; orange: He with C wall; blue: D with Be-W wall). Crosses (with the same color code) mark the disruptions. The straight black line is the bisector y=x.

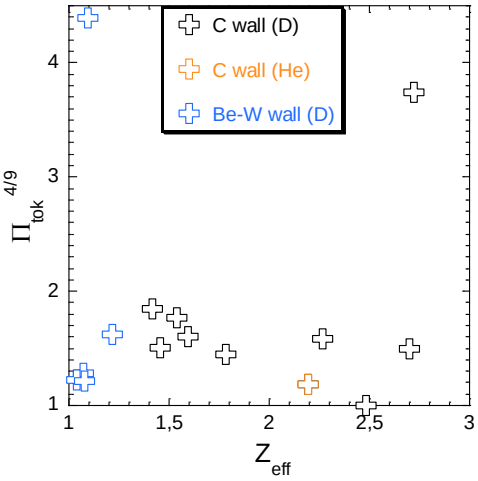

FIG. 2. Estimate of factor $\Pi_{tok}^{4/9}$ *of scaling (10) versus measured* Z_{eff}*. Same color code as figure 1. The two highest crosses refer to shots 59648 (black) and 87494 (blue), having NBI injected power, >10 MW, largely exceeding the ohmic input.*

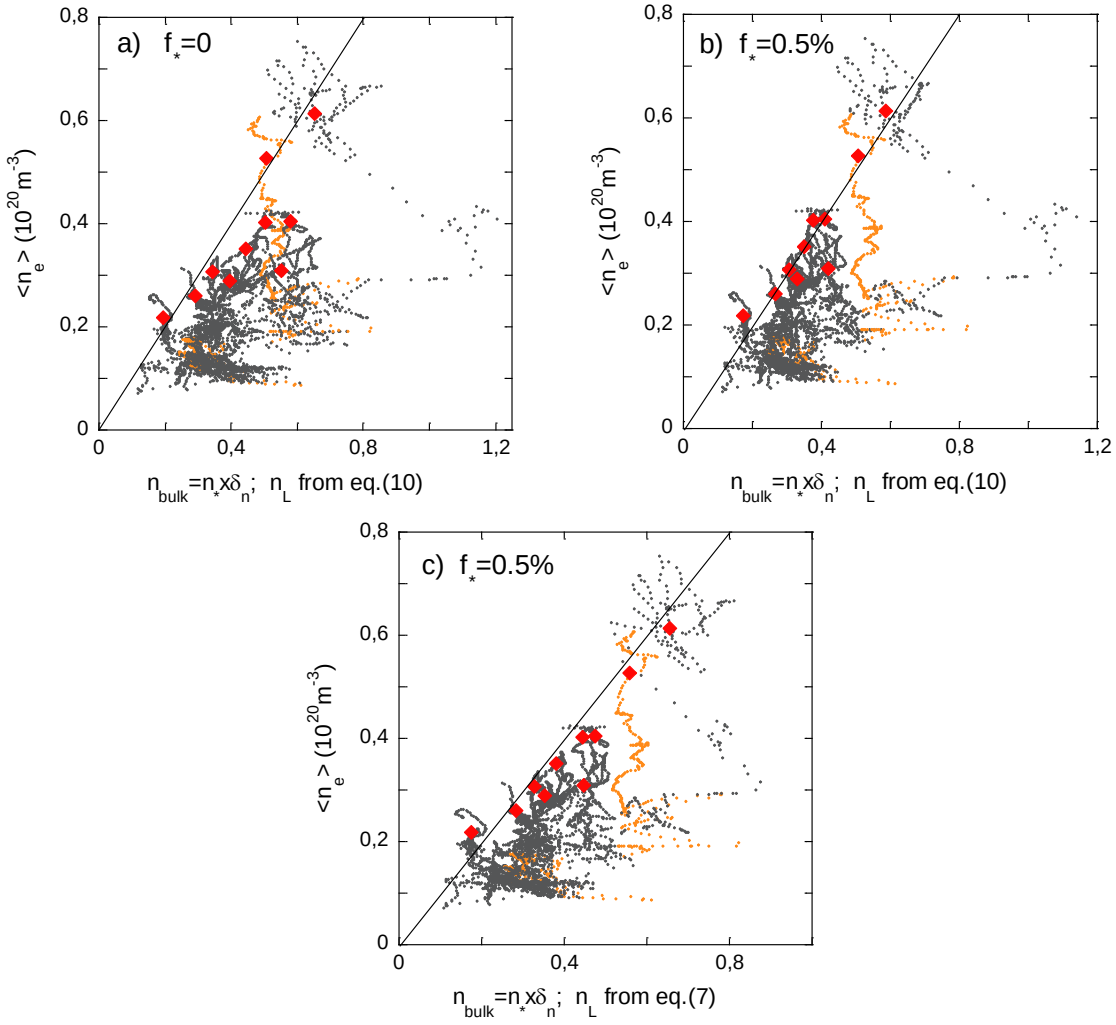

FIG. 3. C wall discharges: experimental densities versus modelled DL, with n_L *given by (10) (a, b) and (7) (c). No neutrals in (a), but* $f_{0*} = 0.005$ *in (b, c). Full traces are reported: in grey D shots, in orange He shot. The y=x bisector is plotted in black. Red diamonds represent the average taken in a 1s time interval close to the disruption.*

4. C WALL DISCHARGES

Visible spectroscopy shows that neutral deuterium (D_0) and C are the main contributors to radiation in the SOL region, in L-mode JET discharges with C wall [16]. Therefore, besides edge D_0 (not considered for the He discharge) we take C as dominant impurity, with a smaller fraction of oxygen (O) [14]. Due to the similarity of the two impurities, model output turns out to be almost independent on their relative concentration in the range $\hat{f}_O = f_O/f_C = 0.1 \div 0.5$. Results are thus displayed for $\hat{f}_O = 0.1$ in figure 3. Model predictions without edge D_0 are also presented (figure 3a), because this case is *almost univocal*, being the dependence on $\hat{f}_O$ negligible. The model describes fairly well the upper boundary of the experimental points, as well as the disruptions, regardless of the choice between equations (7), (10) for n_L (in the latter case, ${\tau_E}^{1/9}$ is expressed by the ITER89-P scaling, and $\xi(0)$ is estimated by inversion of equation (9), with $q(0)$ from equilibrium reconstruction). Moreover, the inclusion of D_0 with small f_{0*} (0.5% for all shots, in figures 3b, 3c) improves the comparison. Note that, the He shot aligns fairly well with the D shots. The dependence of modelled DL on f_{0*} is now analysed shot-by-shot. In figure 4, the ratio $(\langle n_e \rangle / n_{bulk})_{disr}$ between experimental and modelled densities, both taken close to the disruption (as red diamonds of figure 3), is plotted against f_{0*} and $Q_*(f_{0*})$, for all the considered D shots. Apart for 43547, where the ratio stays always above one, agreement is found with f_{0*}~0.8% ÷ 2.5%, corresponding to Q_*~0.2 ÷ 1.5: a significant neutral emission at the edge, in qualitative agreement with the above mentioned experimental analyses [16].

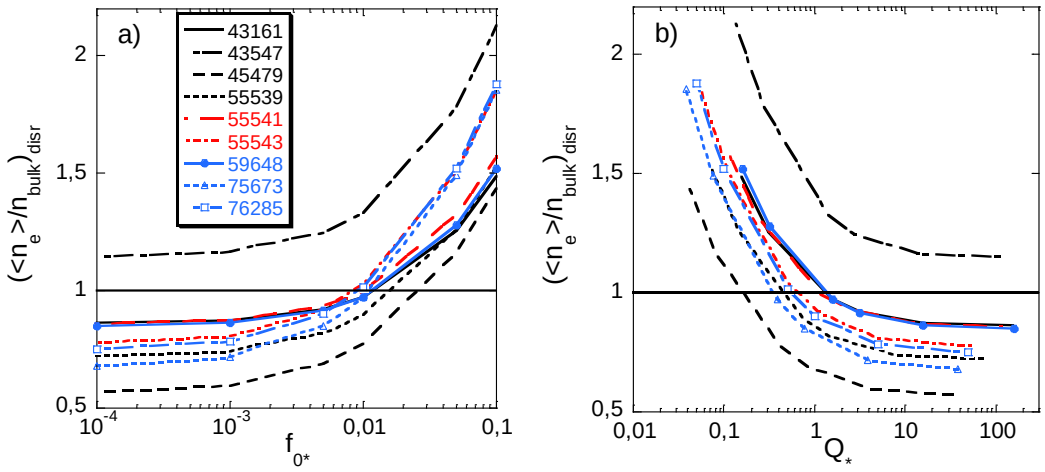

FIG. 4. C wall discharges: shot-by-shot ratio between experimental and predicted DL, versus f_{0*} (a) and Q_* (b). n_{bulk} is computed with n_L from equation (7) and $\hat{f}_O = 0.1$.

5. BE-W WALL DISCHARGES

Typically, neutral deuterium is the main contributor to radiation in the SOL region of L-mode plasmas with Be-W wall [16], owing to the weak radiative loss rate of Be, and the negligible W content (f_W~$1 \div 5 \times 10^{-6}$ is reported). Therefore, the shot-by-shot analysis of the f_{0*} dependence just discussed is repeated in figure 5, with impurity content limited to Be (dominant impurity), and a small fraction of C (we take $\hat{f}_C = f_C/f_{Be} = 0.1$ on the basis of [14]). With the exception of shot 87494, highlighted in red and discussed later, experimental and modelled DL match for f_{0*}~0.5% ÷ 2%, corresponding to Q_*~0.05 ÷ 0.6. The f_{0*} range is similar to that found for C wall discharges, whereas the Q_* interval is shifted towards smaller values, in agreement with the experimentally observed prevalence of D_0 radiation. The off-trend discharge 87494 requires f_{0*}~10% to be reconciled with the model. However, having this shot by far the highest (NBI) power within the present Be-W database, it is possible that a small amount of W, coming from the divertor plates, should be included here. Therefore, in figure 6 the dependence of $(\langle n_e \rangle / n_{bulk})_{disr.}$ on $\hat{f}_W = f_W/f_{Be}$ is displayed for this discharge, for two fixed values, 0.5%, 1%, of f_{0*}. Two different estimates of Rad_W are used. The first, reported in [9], features a peak at T~$2eV$, orders of magnitude larger than the maximum loss rate of any light impurity. The second, reported in [17], is truncated for $T < 30eV$, where atomic data are considered uncertain: in the present analysis *it is set to zero in this temperature interval*. Therefore, the two implemented Rad_W correspond to opposite hypotheses on the W edge emission: respectively very large and negligible. Accordingly, a strong dependence on $\hat{f}_W$ is found when using Rad_W from [9]: agreement between experimental and modelled DL is recovered for very small values of $\hat{f}_W$

($\hat{f}_W \sim 0.003$). Instead, the other choice for Rad_W relaxes to a good extent this dependence, giving $(\langle n_e \rangle / n_{bulk})_{disr.} = 1$ for $\hat{f}_W \sim 0.03$.

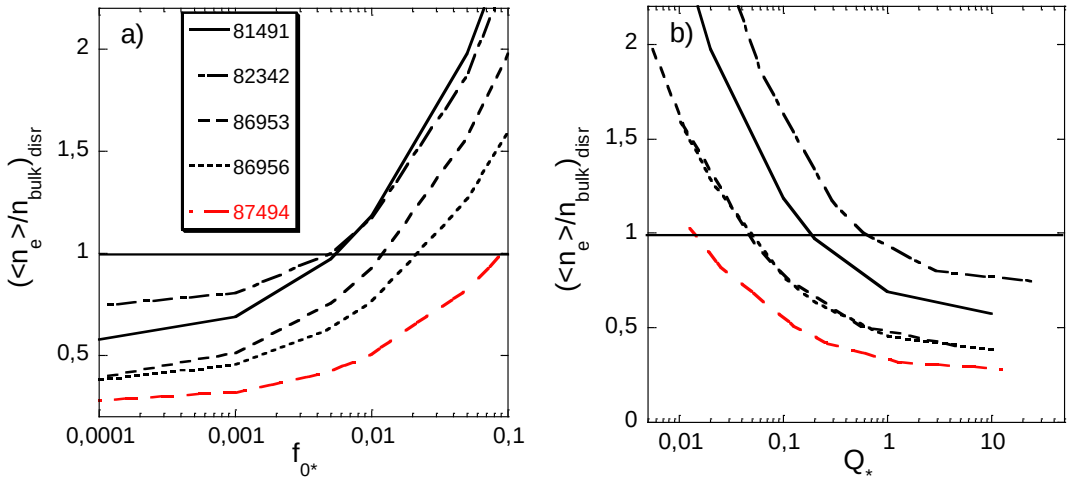

FIG. 5. Same analysis as figure 4 for Be-W wall discharges.

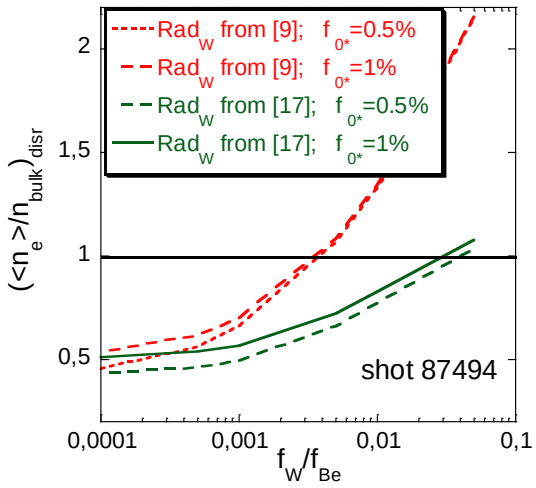

FIG. 6. DL dependence on W (relative) concentration for shot 87494.

6. CONCLUSIONS

A set of high-density disrupted-L-mode JET discharges has been compared with a slightly refined version of the power-balance model presented in [7], where losses are due to radiation from impurities and edge neutrals. Two DL scaling laws, involving equations (7) and (10) respectively, are employed. These equations feature a similar dependence on heating power and current: for (7), it is approximately $P^{0.5} I_p^{0.3}$; for (10), it is $\left(P/V_\phi\right)^{4/9} I_p^{4/9}$, reducing to $I_p^{8/9}$ for an ohmic configuration. These dependences are compatible with those reported in previous publications on L-mode experiments [3, 4]. Both scaling laws agree fairly well with the upper boundary of the observed densities, taking reasonable values of the input parameters, most of which derive from measurements or atomic physics estimates. In particular, specific loss rates of impurities and neutrals, as well as impurities' charges, are taken from database [9] and reference [17]. The measured Z_{eff} provide a sort of average impurities' concentration, but the relative impurities' concentrations, as well as the edge neutrals concentration, are more uncertain parameters. For C wall discharges, inclusion of neutrals' radiation, though improving the comparison with experiments, is not essential, given the significant C emission. Moreover, model's output dependence on

relative O, C concentration is negligible. Hence, this case provides the most convincing model's validation. Instead, neutrals provide the main loss channel in Be-W discharges. Therefore, nothing more than a compatibility assessment with the experiment can be done in this case, within a reasonable range of neutrals' concentration. We also point out the complete inadequacy of the *pure* n_G criterion as a tool to interpret the maximum densities observed shot-by-shot in the present database. Generally speaking, it is true that none of the disruptions occurs at $\langle n_e \rangle > n_G$ (values close to n_G are attained in a couple of shots), but this seems incidental, since other experiments have overcome n_G by high power [18], or by density profile peaking [19].

ACKNOWLEDGEMENT

We thank P. Vincenzi for providing the NBI shine-through signals, and M. Valisa for helpful discussions. This work has been carried out within the framework of the EUROfusion Consortium and has received funding from the Euratom research and training programme 2014-2018 under grant agreement No 633053. The views and opinions expressed herein do not necessarily reflect those of the European Commission.

REFERENCES

[1] S. Sudo et al, Scalings of energy confinement and density limit in stellarator/heliotron devices, Nucl. Fusion **30** (1990) 11

[2] M. Greenwald, Density limits in toroidal plasmas, Plasma Phys. Contr. Fusion **44** (2002) R27

[3] A. Stabler et al, Density limit investigations on ASDEX, Nucl. Fusion **32** (1992) 1557

[4] G. Duesing and the JET Team, First results of neutral beam heating on JET, Plasma Phys. Contr. Fusion **28** (1986) 1429

[5] A.Huber et al, The effect of the isotope on the H-mode density limit, Nucl. Fusion **57** (2017) 086007

[6] M. Bernert et al, The H-mode density limit in the full tungsten ASDEX Upgrade tokamak, Plasma Phys. Contr. Fusion **57** (2015) 014038

[7] P. Zanca et al, A unified model of density limit in fusion plasmas, Nucl. Fusion **57** (2017) 056010

[8] P. Zanca et al, L-mode density limit analyses in JET and TCV, internal document NT-FC/91, RFX, Padova (2018)

[9] Atomic Molecular Data Services, https://www-amdis.iaea.org/FLYCHK/

[10] J. Freidberg, 'Plasma Physics and Fusion Energy', Cambridge University Press, New York (2007)

[11] ITER Physics Expert Group on Confinement and Transport et al, Chapter 2: Plasma confinement and transport, Nucl. Fusion **39** (1999) 2175

[12] S. Inagaki et al, Comparison of transient electron heat transport in LHD helical and JT-60U tokamak plasmas, Nucl. Fusion **46** (2006) 133

[13] S. Cappello, D. Bonfiglio, D. F. Escande, Magnetohydrodynamic dynamo in reversed field pinch plasmas: Electrostatic drift nature of the dynamo velocity field, Phys. Plasmas **13** (2006) 056102

[14] S. Brezinsek et al, Plasma-surface interaction in the Be/W environment: Conclusions drawn from the JET-ILW for ITER, J. Nucl. Mater. **463** (2015) 11-21

[15] K. Thomsen et al, ITER H mode confinement database update, Nucl. Fusion **34** (1994) 131

[16] M. Groth et al, Impact of carbon and tungsten as divertor materials on the scrape-off layer conditions in JET, Nucl. Fusion **53** (2013) 093016

[17] T. Putterich et al, Calculation and experimental test of the cooling factor of tungsten, Nucl. Fusion **50** (2010) 025012

[18] J. Rapp et al, Density limits in TEXTOR-94 auxiliary heated discharges, Nucl. Fusion **39** (1999) 765

[19] G. Pucella et al, Density limit experiments on FTU, Nucl. Fusion **53** (2013) 083002